Available online at www.sciencedirect.com
SCIENCE DIRECT®
Journal of Solid State Chemistry 173 (2003) 395–406
JOURNAL OF SOLID STATE CHEMISTRY
http://elsevier.com/locate/jssc

Synthesis and structural studies of $Sr_2Co_{2-x}Ga_xO_5$, $0.3 \leqslant x \leqslant 0.8$

F. Lindberg,[a] S.Ya. Istomin,[b] P. Berastegui,[a] G. Svensson,[a,*] S.M. Kazakov,[c] and E.V. Antipov[b]

[a] *Departments of Structural and Inorganic Chemistry, Stockholm University, Stockholm SE-10691, Sweden*
[b] *Department of Chemistry, Moscow State University, Moscow 119899, Russia*
[c] *Lab. Fuer Festkoerperphysik, ETH Hönggerberg, Zürich CH-8093, Switzerland*

Received 22 October 2002; received in revised form 12 February 2003; accepted 20 February 2003

Abstract

The novel oxide $Sr_2Co_{2-x}Ga_xO_5$ with brownmillerite-type structure has been synthesized in the compositional range $0.3 \leqslant x \leqslant 0.8$. Rietveld refinements using neutron powder diffraction data have been performed for the end compositions, $x = 0.3$ and 0.8. The structure is best described in the space-group *Icmm* (no. 74) with unit cell parameters $a = 5.5678(6)$, $5.6126(7)$ Å, $b = 15.749(2)$, $15.733(2)$ Å and $c = 5.4599(6)$, $5.4559(7)$ Å for the $x = 0.3$ and 0.8 compositions, respectively. The compounds were found to be G-type antiferromagnetic with the magnetic moments parallel to the *c*-axis. High-temperature magnetic susceptibility measurements confirmed the samples to be antiferromagnetic with Néel temperatures $T_N = 505$, 468 and 423 K for the $x = 0.3$, 0.5 and 0.8 samples, respectively. High-resolution transmission electron microscopy and electron diffraction studies confirmed the I-centred structure and revealed the presence of disorder.

Keywords: Complex cobalt oxides; Brownmillerite structure; Neutron powder diffraction; Electron diffraction

1. Introduction

The flexibility of the perovskite structure makes it possible to change the physical properties by introducing anion vacancies and mixed valence states at the cation positions. These anion vacancies may order and superstructures are then formed that are intergrowths between perovskite and oxygen deficient perovskite layers. One important superstructure is the brownmillerite-type structure (Ca_2FeAlO_5 [1,2]) often found for $A_2B_2O_5$ compounds. In this structure, the oxygen vacancies are ordered in a way that layers of chains of corner linked BO_4 tetrahedra are formed, see Fig. 1. The brownmillerite structure can thus be described as consisting of alternating layers of BO_6 octahedra and BO_4 tetrahedra. The resulting unit cell relations between the perovskite and brownmillerite structure are $a \approx c \approx a_p \times \sqrt{2}$ and $b \approx 4 \times a_p$ (a_p—ideal cubic perovskite structure).

The relative orientation of the tetrahedra between the layers can give rise to two ordered structures having space groups *Ibm*2 (no. 46) and *Pcmn* (no. 62) as shown in Fig. 1. In the former, the chains of tetrahedra are oriented in phase (b), while they are out of phase in the latter (c). Very often a third variant is found crystallizing in space group *Icmm* (no. 74) (d). It represents incomplete ordering within the tetrahedral layers with partially filled atomic positions in the tetrahedral chain. It has also been shown in some brownmillerite-type compounds that ordering of the tetrahedral chains occur giving rise to features such as diffuse scattering and satellite reflexes in reciprocal space [3,4].

The brownmillerite-type structure can often be stabilized by introducing different cations at the octahedral and tetrahedral positions such as in the recently reported $Sr_2MnGaO_{5+\delta}$, [5,6] and $Ca_2MnGaO_{5+\delta}$ [7]. The ordering of the chains of tetrahedra in brownmillerite-type compounds has been proposed to be influenced by the ionic size of the doping cation [6]. However, it is difficult to distinguish between the different variants using diffraction methods, e.g. for $Sr_2MnGaO_{5+\delta}$ space groups *Icmm* [6] and *Ibm*2 [5] have been proposed.

Among complex cobalt oxides with cobalt in oxidation state +3 only, the compound $Sr_2Co_2O_5$ with

*Corresponding author. Fax.: +46-8-163118.
E-mail address: gunnar@struc.su.se (G. Svensson).

0022-4596/03/$ - see front matter © 2003 Elsevier Science (USA). All rights reserved.
doi:10.1016/S0022-4596(03)00129-4

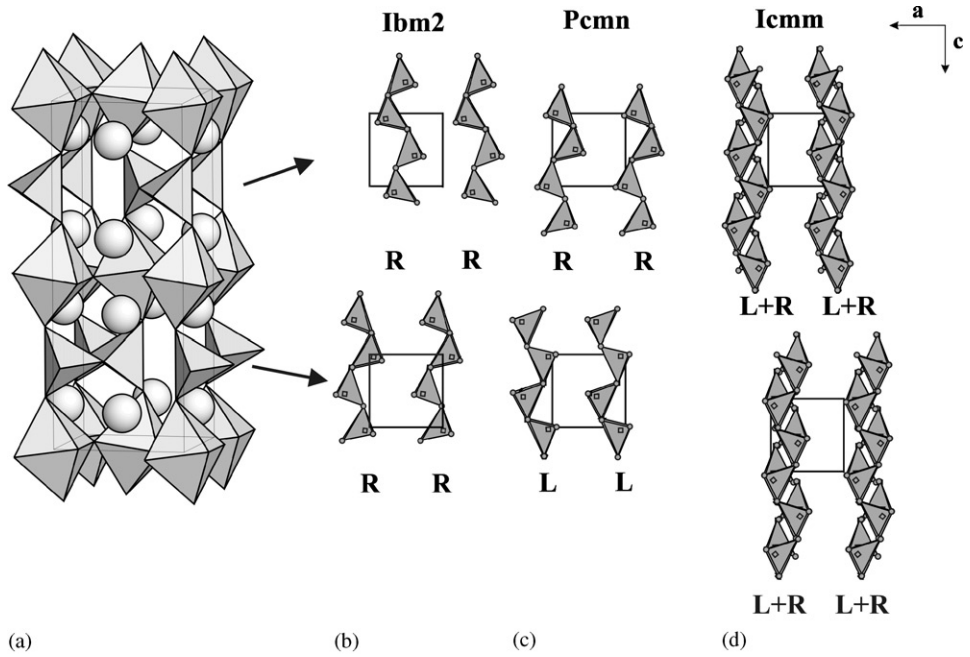

Fig. 1. Crystal structure of brownmillerite in space group *Ibm*2 (a) and corresponding orientation of the tetrahedral chains in the structure (b). For a comparison the orientation of the tetrahedral chains in space groups *Pcnm* (c) and *Icmm* (d) is given. Note that in *Ibm*2 the orientation of the chains is in phase in both tetrahedral layers while they are out of phase in *Pcnm*. *Icmm* represents incomplete ordering of the chains in both layers.

brownmillerite-type structure has been known for a long time [8]. However, this compound is stable in air atmosphere only above $T = 1200\,K$ and can be prepared by quenching [9]. Below $T = 1200\,K$ $Sr_2Co_2O_5$ decomposes to $Sr_6Co_5O_{15}$ [10] and Co_3O_4 upon slow cooling. The instability is in this case most probably caused by the presence of Co^{3+} ($3d^6$) in an unstable tetrahedral coordination. The existence of a brownmillerite cobaltate with tetrahedrally coordinated cobalt has been attributed to the stabilization of the high spin state for cobalt at elevated temperatures [9]. Thus, a way to stabilize the brownmillerite structure would be to substitute part of the Co^{3+} by a trivalent cation with a preference for tetrahedral coordination.

In this paper we present a study of the system $Sr_2Co_{2-x}Ga_xO_5$. The stability range of the brownmillerite structure has been studied using X-ray powder diffraction. The crystallographic structure has been investigated using high-resolution electron microscopy, electron diffraction and X-ray and neutron powder diffraction techniques. The magnetic properties of the compounds have also been determined.

2. Experimental

Samples of $Sr_2Co_{2-x}Ga_xO_5$ with Ga content $0.0 \leqslant x \leqslant 1.0$, $\Delta x = 0.1$, were synthesized from stoichiometric mixtures of $SrCO_3$, Ga_2O_3 and Co_3O_4. The mixtures were carefully grinded and sintered in air at 1373 K for 24 h followed by re-grinding and further firing at 1373 K for 72 h. Thereafter the furnace was shut off and samples cooled down to room temperature. Phase analysis of the products was made by means of their X-ray powder diffraction photographs recorded using a Guinier-Hägg camera with focusing geometry using Cu$K\alpha_1$ radiation and Si as internal standard.

X-ray powder diffraction data for Rietveld refinements were collected for the samples $x = 0.3$ and 0.8 on a STOE STADI-P diffractometer in the symmetric transmission mode and a linear position sensitive detector (mini-PSD) covering 4.6° in 2Θ. Room temperature neutron powder diffraction data were collected at the NPD instrument at the Swedish research reactor, NFL, Studsvik. The wavelength of the neutrons was 1.47 Å. The sample was placed in a can of thin vanadium foil. Data were collected between the 2θ range 4.00–139.92° with a step length of 0.08°. Refinement of the nuclear and magnetic structures was done using the GSAS suite of programs [11]. The background and the peak shape were modeled by a Chebyschev polynom and a Gaussian profile function, respectively. The neutron scattering lengths were taken from the GSAS library.

For transmission electron microscopy studies small amounts of the samples were crushed in *n*-butanol. A drop of this dispersion was put on a holey carbon film supported by a copper grid. Electron diffraction studies (ED) and microanalysis were made in a JEOL JEM2000 FX instrument operated at 200 kV equipped with a LINK AN10000 energy-dispersive X-ray microanalysis (EDX) system. High-resolution electron microscopy

studies were made in a JEOL JEM3010 UHR microscope operated at 300 kV. Additional EDX analysis for the determination of cation content on the same grids as studied in the TEM were performed with a JEOL JSM 880 scanning electron microscope equipped with a windowless energy-dispersive analyzer (EDS) LINK *Isis*. Simulated HREM images were calculated using MacTempas [12].

Iodometric titration was used to determine the oxygen content in the as-prepared samples with $0.3 \leqslant x \leqslant 0.8$. About 50 mg of the sample under investigation was placed in a flask containing 20 ml of a 20% water solution of KI. Then, several drops of concentrated HCl were added to the solution. The flask was kept in a dark place until the entire sample had dissolved. The released elementary iodine was titrated by a standard $Na_2S_2O_3$ solution with starch added as an indicator.

The high-temperature magnetic measurements were performed by the Faraday method in a field of 5 kOe from 25°C up to 700°C.

3. Results

After annealing the color of the samples was black. The XRD study revealed that monophasic samples were obtained for $0.3 \leqslant x \leqslant 0.7$. In the $x = 0.8$ sample small amounts of a strontium gallate phase ($Sr_3Ga_4O_9$ [13]) was detected. A large amount of this impurity phase was found in the samples with $x \geqslant 0.9$ while at $x \leqslant 0.2$ strong lines from $Sr_6Co_5O_{15}$ could be seen. The unit-cell parameters for the samples with $0.3 \leqslant x \leqslant 0.8$ are listed in Table 1, where a small increase of the *a*-axis with increasing gallium content can be observed. Examination of the 200, 141 and 002 reflections of the prepared compounds, which are derived from the 110 perovskite substructure reflection, shows that the orthorhombic distortion slightly increases with increasing gallium content, as seen in Fig. 2. The EDS analysis of the cations in both the TEM and SEM were in agreement with the nominal composition.

The oxygen content remained stoichiometric within 2 e.s.d. for all compositions; e.g. the oxygen content, as determined by iodometric titration, for the $x = 0.3$ sample corresponds to the formula $Sr_2Co_{1.7}Ga_{0.3}O_{5.04(2)}$. Annealing of the $0.3 \leqslant x \leqslant 0.8$ samples in air at 1173 K

Table 1
Unit cell parameters (Å) for $Sr_2Co_{2-x}Ga_xO_5$, $0.3 \leqslant x \leqslant 0.8$

x	*a*	*b*	*c*
0.3	5.592(2)	15.729(4)	5.466(1)
0.4	5.586(2)	15.758(4)	5.461(2)
0.5	5.592(4)	15.746(9)	5.462(3)
0.6	5.607(3)	15.751(5)	5.546(2)
0.7	5.611(3)	15.741(6)	5.455(3)
0.8	5.626(1)	15.739(4)	5.454(1)

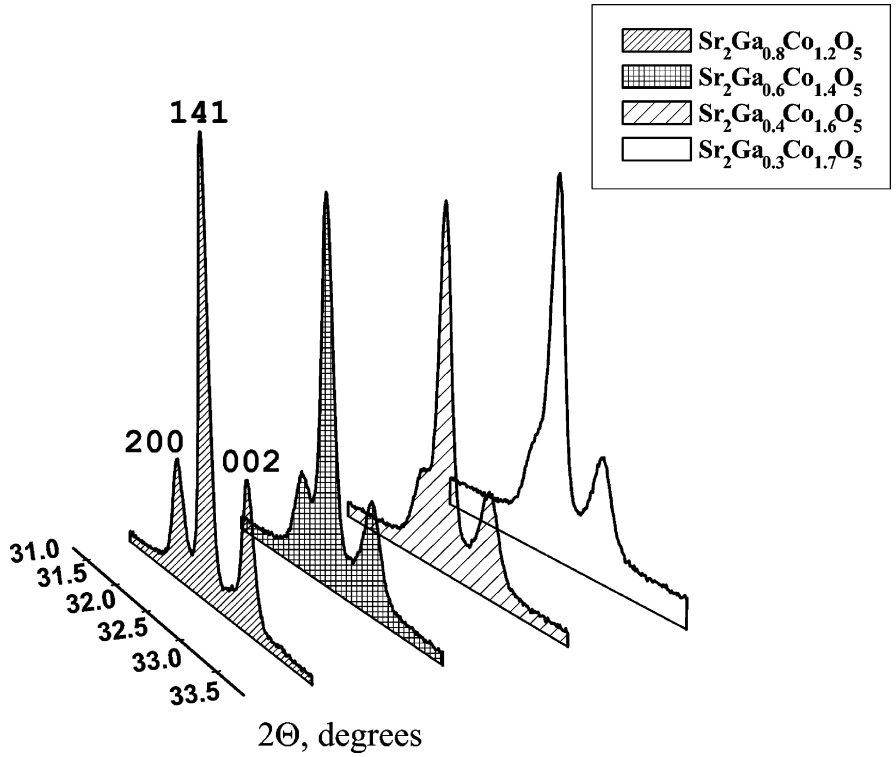

Fig. 2. X-ray powder diffraction patterns of the main reflections 200, 141 and 002 for the $Sr_2Co_{2-x}Ga_xO_5$, $x = 0.8$, 0.6, 0.4, 0.3 showing an increasing difference between *a* and *c* parameters with increasing gallium content.

Table 2
Néel temperatures (T_N), Curie (C), Weiss (Θ) constants and effective magnetic moments (μ_{eff}) per cobalt atom for $Sr_2Co_{2-x}Ga_xO_5$, $x = 0.3$, 0.5 and 0.8. C, Θ and μ_{eff} were obtained by linear fitting of $1/\chi$ versus T between Néel temperature and 650 K

x	T_N,/K	C	Θ	μ_{eff},/μ_{BM}
0.3	505	6.7(1)	−1651(38)	5.6(1)
0.5	468	5.10(5)	−1326(18)	5.2(1)
0.8	423	2.91(3)	−740(13)	4.41(7)

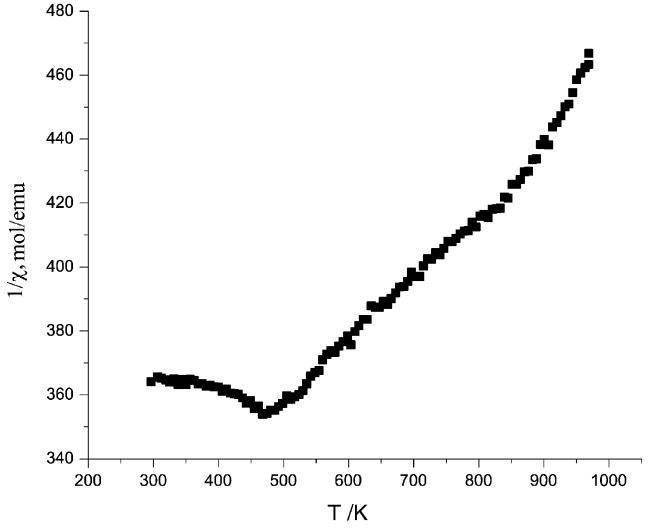

Fig. 3. Temperature dependence of the inverse molar magnetic susceptibility for $Sr_2Co_{1.5}Ga_{0.5}O_5$.

for 72 h revealed that the brownmillerite phase is not stable and decomposes into $Sr_6Co_5O_{15}$, Co_3O_4 and strontium gallates.

The magnetic susceptibility data for $Sr_2Co_{2-x}Ga_xO_5$, $x = 0.3$, 0.5 and 0.8 indicate the compounds to be antiferromagnetic with Néel temperatures above 400 K, see Table 2. The reciprocal magnetic susceptibility versus temperature exhibit a Curie–Weiss behavior $\chi = C/(T-\theta)$ above the Néel temperature for all three sample, as shown for $x = 0.5$ in Fig. 3. The magnetic moments, Curie and Weiss constants in Table 2 were obtained by linear fitting of the data in the temperature range from Néel temperature to 650 K.

3.1. XRD and NPD studies

The XRD and the NPD data revealed the systematic absences $h\,k\,l$: $h+k+l=2n+1$ and $0\,k\,l$: k, $l = 2n+1$ in agreement with the space groups $Ibm2/Icmm$. The I-centring was also supported by the ED studies, see below. An idealized structure model of brownmillerite was used as a starting model for the refinements. No reflections from admixture phases were found in the XRD patterns of $Sr_2Co_{2-x}Ga_xO_5$, $0.3 \leqslant x \leqslant 0.7$, while several weak reflections (max intensity 2%) from $Sr_3Ga_4O_9$ [13] were detected in the XRD pattern of the $x = 0.8$ sample. Careful examination of the reflection profiles of all samples except $x = 0.8$ showed that the half-width of the reflection 2 0 0 (FWHM = 0.25) was about 50% larger than the neighboring 1 4 1 reflection (FWHM = 0.17°). As an example, fitting of the 2 0 0,

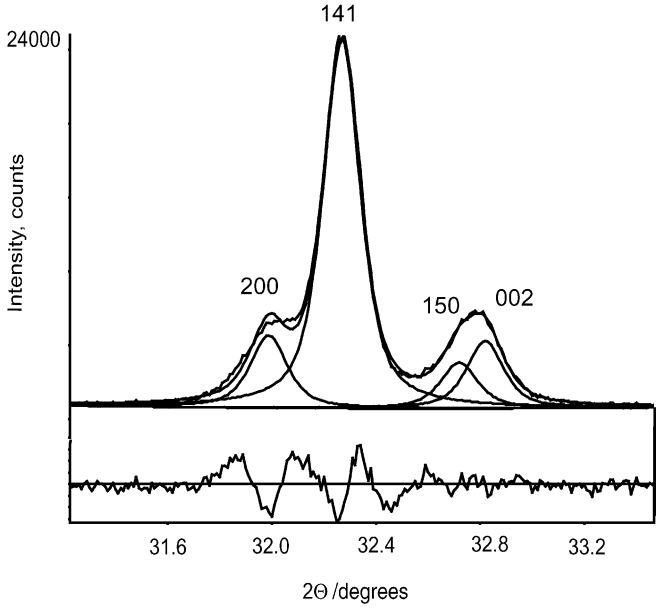

Fig. 4. Fitting of the profile of 2 0 0, 1 4 1 and 0 0 2 reflections for $Sr_2Co_{2-x}Ga_xO_5$ $x = 0.6$ with fixed FWHM = 0.17°. Note the poor fitting of the 2 0 0 reflection indicating that the FWHM is much higher than for the neighboring 1 4 1 reflection.

Table 3
Summary of the results of the least-square fits to the neutron powder diffraction data collected for $Sr_2Co_{2-x}Ga_xO_5$, $x = 0.3$ and 0.8

x	0.3	0.8
Space group (space group for the magnetic structure)	*Icmm* (*Icm′m′*)	*Icmm* (*Icm′m′*)
Lattice parameters (Å):	$a = 5.5768(6)$	$a = 5.6126(7)$
	$b = 15.749(2)$	$b = 15.733(2)$
	$c = 5.4599(6)$	$c = 5.4559(7)$
χ^2	1.94	1.86
R_F^2	0.0477	0.0398
R_{wp}	0.0441	0.0430
R_p	0.0340	0.0334
Number of reflections (Bragg and magnetic), N_p	1685	1685
Number of fitted parameters, N_f	39	41

Atom	Wy. site	x	y	z	$U^*_{iso}100/Å^2$	Magnetic moment per site	Magnetic moment per Co	Occ.
$x = 0.3$								
Sr	8*h*	0.0115(7)	0.1118(1)	0.5	0.62(7)			1
Co1/Ga1	4*a*	0	0	0	0.7(2)	2.77(5)	2.86	0.97/0.03(1)
Co2/Ga2	8*i*	−0.070(1)	0.25	−0.041(2)	0.4(2)	2.52(8)	3.47	0.363(6)/0.137(6)
O1	8*g*	0.25	−0.0050(3)	0.25	1.09(7)			1
O2	8*h*	0.0425(6)	0.1424(2)	0	1.25(9)			1
O3	8*i*	0.868(1)	0.25	0.624(1)	1.4(2)			0.5
$x = 0.8$								
Sr	8*h*	0.0147(6)	0.1112(1)	0.5	0.69(8)			1
Co1/Ga1	4*a*	0	0	0	1.4(2)	2.32(5)	2.64	0.88/0.12(1)
Co2/Ga2	8*i*	−0.070(1)	0.25	−0.039(2)	0.2(2)	2.0(1)	4.76	0.21/0.29(1)
O1	8*g*	0.25	−0.0064(3)	0.25	1.14(8)			1
O2	8*h*	0.0456(6)	0.1434(2)	0	1.62(9)			1
O3	8*i*	0.864(1)	0.25	0.622(1)	1.5(2)			0.5

1 4 1 and 0 0 2 reflections of the phase with $x = 0.6$ is given in Fig. 4. The experimental profile cannot be adequately described by fitting the reflections with a fixed FWHM = 0.17°. This could be due to the presence of structural disorder caused by different tetrahedral chain ordering as observed in the TEM studies discussed below. Such peculiarities of the profile may be the reason why the refinements of the structures using XRD data for the different samples, $0.3 \leqslant x \leqslant 0.7$, did not proceed well. Several interatomic Co/Ga–O distances were unreasonably short and the thermal parameters for some oxygen atoms were not positively defined.

To obtain reliable structure information, refinements of the crystal structures of the end compositions $x = 0.3$ and 0.8 were performed using NPD data. It was found that the structural models in space group *Pcmn*, did not converge for any of the data sets, which was in agreement with the interpretation of the systematically absent reflections. The combined magnetic and nuclear structure models in *Ibm*2 as well as in *Icmm* refined smoothly and ended in acceptable combined R and χ^2- values, see Table 3. However, the refinement of the structure model in space group *Icmm* resulted in significantly lower values ($x = 0.3(0.8)$ for *Ibm*2 $R_p = 4.17(3.94)$, $\chi^2 = 2.82(2.53)$ and for *Icmm* $R_p = 3.62(3.63)$, $\chi^2 = 2.20(2.21)$) and better I_{obs}–I_{calc}, and will therefore be presented here. Because of the large difference between the neutron scattering powers of Ga (0.7288 barn) and Co (0.249 barn) the relative distribution of Ga and Co in the tetrahedral and the octahedral sites could be satisfactorily refined. The obtained overall Ga composition $x = 0.30$ and 0.70 is in excellent agreement with the nominal composition for the $x = 0.3$ sample, while it is slightly lower for the $x = 0.8$. This is in agreement with the XRD phase analysis which revealed the presence of a small amount of $Sr_3Ga_4O_9$ in the $x = 0.8$ sample. As the Co2/Ga2 and the O3 position in the tetrahedra are split positions these occupancies were set to 0.5. The possibility of a split O2 position, which is the bridging atom between the tetrahedra and the octahedra, was tested as well without success. An isotropic model was used for the temperature factors.

Examination of the NPD patterns for $x = 0.8$ and 0.3 showed the presence of strong reflections from a

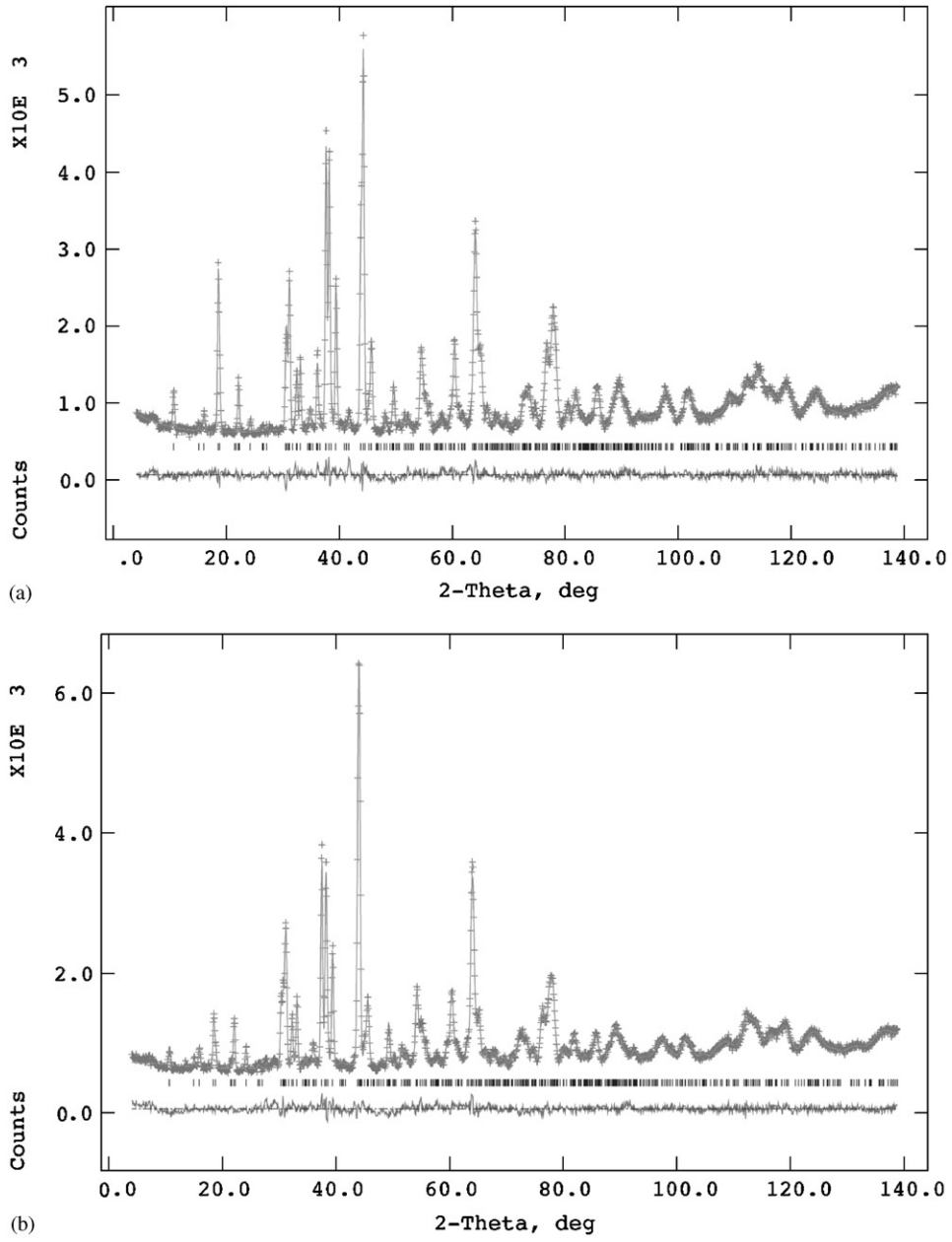

Fig. 5. Observed (crosses), calculated (solid line) and difference (bottom) neutron powder diffraction patterns of $Sr_2Co_{2-x}Ga_xO_5$, (a) $x = 0.3$ and (b) $x = 0.8$ from the final refinement. The tick marks show the calculated positions for the reflections.

magnetic structure. The magnetic space group was $Icm'm'$. A G-type antiferromagnetic (AFM) model where the magnetic moment of all the Co atoms are oriented in the opposite directions relative to the six nearest neighbors was used. The corresponding refined magnetic moments μ_{eff}/μ_{BM} for the Co1 and Co2 cations were 2.77(5), 2.52(8) and 2.32(5), 2.0(1) for the $x = 0.3$ and 0.8 sample, respectively. The magnetic moments for both Co cations in both structures are oriented parallel to [001]. The final values of the fitted atomic parameters are given in Table 3 and I_{obs} and I_{obs}–I_{calc} curves for both $x = 0.3$ and 0.8 are shown in Fig. 5. Selected interatomic distances and angles are given in Table 4.

3.2. Transmission electron microscopy studies

The ED studies of the brownmillerite crystallites revealed both ordered and disordered crystallites. The symmetry and extinction conditions in the ED patterns of the brownmillerite crystallites are in agreement with the neutron powder diffraction data. The reflection conditions $0\,k\,l$, with $k + l = 2n$ and $l = 2n$ and $h\,k\,0$, with $h + k = 2n$ in the SAED $[100]_{BM}$ and the $[001]_{BM}$ (BM—brownmillerite-type) zone axis patterns, shown in Fig. 6a and b, respectively, confirms an I centred space group and a glide plane normal to the a-axis, in agreement with the space groups $Icmm$ and $Ibm2$ found

Table 4
Selected interatomic distances (Å) and angles (°) for $Sr_2Co_{2-x}Ga_xO_5$

Distances (Å)			Angles (°)		
(a) $x=0.3$					
Octahedron					
O1–Co1/Ga1	(×4)	1.9527(2)	O1–Co1/Ga1–O1	(×2)	88.7(1)
O2–Co1/Ga1	(×2)	2.254(3)		(×2)	91.3(1)
			O2–Co1/Ga1–O1	(×4)	88.0(2)
				(×4)	92.0(2)
Tetrahedron[a]					
O2–Co2/Ga2	(×2)	1.821(4)	O2–Co2/Ga2–O2		137.3(6)
O3–Co2/Ga2		1.87(1)	O2–Co2/Ga2–O3	(×2)	104.5(3)
		1.881(9)		(×2)	100.2(4)
			O3–Co2/Ga2–O3		107.6(5)
Strontium					
Sr–O1	(×2)	2.648(4)			
	(×2)	2.611(4)			
Sr–O2		2.7775(7)			
		2.535(5)			
		3.126(5)			
Sr–O3		2.417(4)			
(b) $x=0.8$					
Octahedron					
O1–Co1/Ga1	(×4)	1.9594(3)	O1–Co1/Ga1–O1	(×2)	88.23(2)
O2–Co1/Ga1	(×2)	2.271(3)		(×2)	91.77(2)
			O2–Co1/Ga1–O1	(×4)	88.3(1)
				(×4)	91.70(1)
Tetrahedron[a]					
O2–Co2/Ga2	(×2)	1.812(4)	O2–Co2/Ga2–O2		135.5(5)
O3–Co2/Ga2		1.88(1)	O2–Co2/Ga2–O3	(×2)	105.2(3)
		1.867(7)		(×2)	100.7(3)
			O3-Co2/Ga2-O3:		106.9(4)
Strontium					
Sr–O1	(×2)	2.651(4)			
	(×2)	2.605(4)			
Sr–O2	(×2)	2.7800(8)			
		2.519(5)			
		3.186(5)			
Sr–O3		2.435(4)			

[a] Interatomic distances to only in one of the split positions for Co2/Ga2 and O3 are given.

in the NPD study discussed above. The SAED and HREM images frequently revealed that the crystallites consisted of differently oriented brownmillerite domains with a common perovskite subcell direction. An HREM image of two such domains viewed along $[100]_{BM}$ and $[001]_{BM}$ with the common perovskite axis $\langle 110\rangle_p$, are shown in Fig. 7. There is no sharp boundary between the different domains indicating that the viewing direction is not parallel to the domain boundary plane. A simulated HREM image (defocus = −600 Å, thickness = 40 Å) calculated using the atomic coordinates from the $x=0.3$ in Table 3 is inserted in each domain in the image. There is a good correspondence between the simulated and observed HREM image. The $[001]_{BM}$ and $[100]_{BM}$ domains were often also intergrown with the third $\langle 110\rangle_{pp}$ direction in the brownmillerite-type structure $[212]_{BM}$, as seen in the HREM image shown in Fig. 8. The corresponding $[212]_{BM}$ zone axis SAED pattern is shown in Fig. 9. The SAED patterns of brownmillerite viewed along this direction are difficult to distinguish from the $\langle 110\rangle_p$ patterns of ideal perovskite, as only the perovskite subcell reflections are seen. One way to distinguish between brownmillerite and the ideal perovskite structure is to tilt 18° around the $\langle 110\rangle_p = [10\bar{1}]_{BM}$ subaxis to the $[111]_{BM} = \langle 012\rangle_p$ zone axis pattern of brownmillerite. In the cases when this was made, it was confirmed that the domains had brownmillerite-related structures. In many of the $[212]_{BM} = \langle 110\rangle_p$ zone axis patterns weak satellite reflections could be observed at

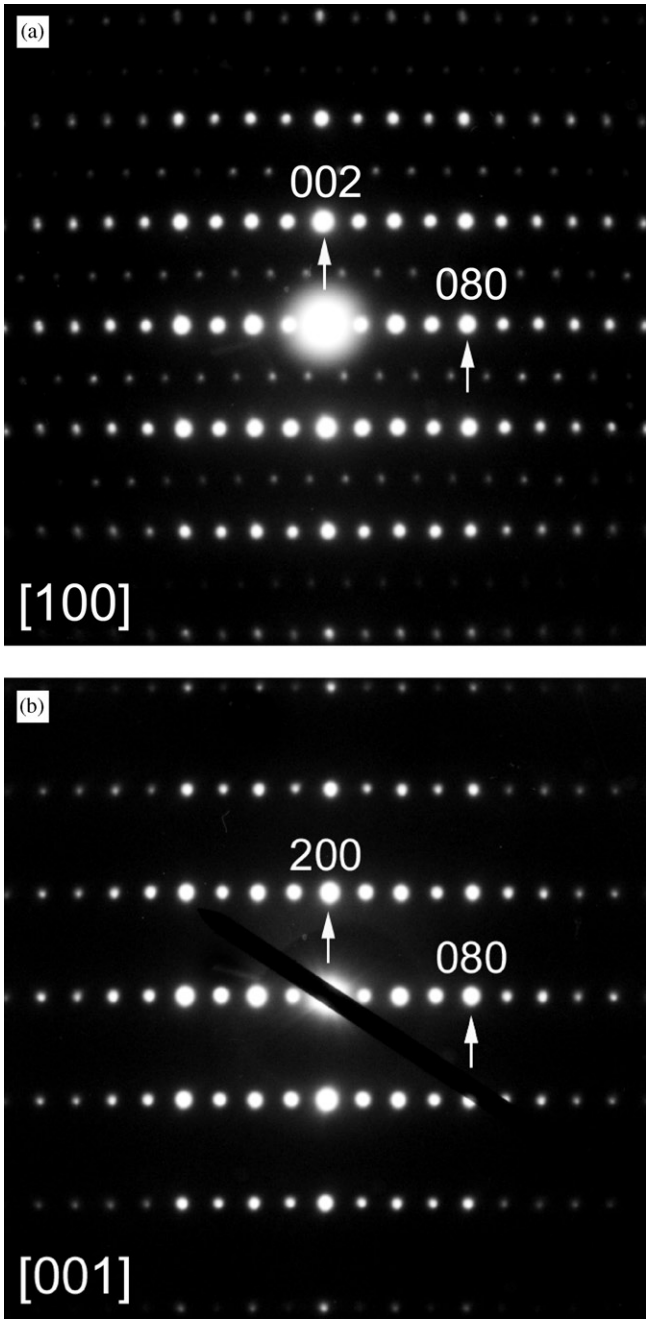

Fig. 6. Selected area diffraction patterns of brownmillerite-type $Sr_2Co_{2-x}Ga_xO_5$, $x = 0.3$ viewed along (a) [100] and (b) [001].

$\mathbf{q} = \frac{1}{4}\langle 111 \rangle^*_p = \frac{1}{4}[04\bar{2}]^*_{BM}$, e.g. in Fig. 9. Their origin can be seen as a weak modulation in the $\langle 212 \rangle_{BM}$ domain shown in Fig. 8. The intensity of these satellite reflections varied within and between the different domains. A HREM image of an area with very strong modulation can be seen in Fig. 10. The FFT of the encircled area show that the modulation is well ordered and can be described as a quadrupling along $[04\bar{2}]_{BM} = \langle 111 \rangle_p$. In the range shown there is a twin boundary in the modulations, with a mirror plane parallel to $\{100\}_p = \{101\}_{BM}$.

It should also be mentioned that we frequently observed streaking in the SAED patterns. For example the $[20\bar{1}]_{BM}$ zone axis pattern ($[103]_p$) reveal lines of streaking along $\langle 010 \rangle^*_{BM}$ sited at $\mathbf{q} = \frac{1}{4} \pm \langle 402 \rangle^*_{BM}$, as shown in Fig. 11. In the lines there are intensity maxima indicating some preferred ordering. This phenomen has often been observed in brownmillerites, see e.g. [3,4,14], and has been attributed to disorder within the tetrahedral layers. This would explain the lower *R*-values obtained in the refinements of $Sr_2Co_{2-x}Ga_xO_5$ using the *Icmm* space group.

4. Discussion

Complex cobalt oxides $Sr_2Co_{2-x}Ga_xO_5$, $0.3 \leqslant x \leqslant 0.8$ with a brownmillerite-type structure can be successfully synthesized in the experimental conditions used, while $Sr_2Co_2O_5$ needs fast quenching. However, prolonged annealing of the samples at 1173 K revealed that they are not stable and decompose as observed for $Sr_2Co_2O_5$ at a slightly higher temperature. Substitution of the Co^{3+} by Ga^{3+} seems to stabilize the brownmillerite structure by decreasing the rate of the decomposition process only.

In $Sr_2Co_{2-x}Ga_xO_5$, $0.3 \leqslant x \leqslant 0.8$ only small changes of the unit cell parameters is observed with increasing Co^{3+} content, due to the similar ionic radii 0.61 Å of high spin Co^{3+} and Ga^{3+} [15]. A structure model of the brownmillerite $Sr_2Co_{2-x}Ga_xO_5$ consisting of a tetrahedron and an octahedron is shown in Fig. 12. Atoms in only one of the split positions for Co2/Ga2 and O3 are shown for clarity. The Co1/Ga1 octahedra can be described as 4 + 2 being dilated along the *b*-axis towards the O2 atoms, which are shared with the tetrahedra. The O–Co1/Ga1–O angles are all close to ideal values. The tetrahedron is distorted and stretched along the *b*-axis. This gives longer Co2/Ga2–O2 bonds and larger O2–Co2/Ga2–O2 angles compared to the Co2/Ga2–O3 distances and the O3–Co1/Ga1–O3 angles.

The above-mentioned dilation of the MO_6 octahedra is an important feature of the brownmillerite structure. For example, for Fe^{3+} (d^5) in $Sr_2Fe_2O_5$ [16] and for Mn^{3+} (d^4) in Sr_2MnGaO_5 [5] the equatorial distances are 1.98 Å and 1.91–1.98 Å, while the axial ones are 2.20 and 2.41 Å, respectively. This is similar to that found in $Sr_2Co_{2-x}Ga_xO_5$ (see Table 4). In the process of the transformation of the perovskite structure into brownmillerite one strong distortion of the structure occurs. In comparison with the perovskite structure in the brownmillerite neighboring octahedra layers are connected to each other via tetrahedron (see Fig. 1). Replacing of the octahedra by tetrahedra leads to the compression of the structure since height of the octahedra is not equal

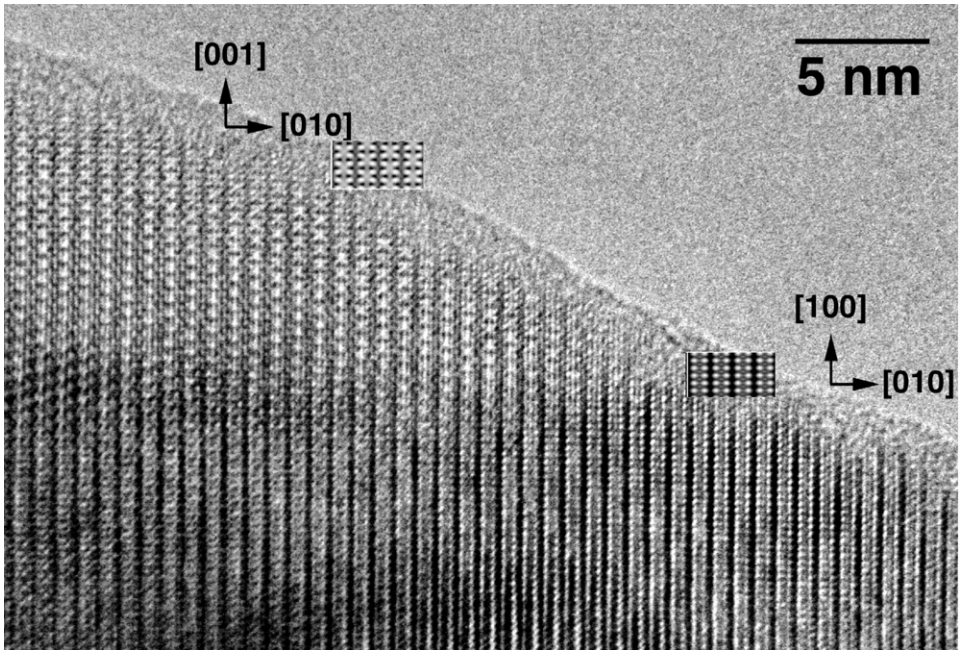

Fig. 7. HREM image of a crystallite of $Sr_2Co_{2-x}Ga_xO_5$, $x = 0.3$ showing two domains of brownmillerite-type structure oriented along the [100] and [001] directions. A simulated HREM image (defocus –600, thickness = 40 Å) using the coordinates in Table 3 is inserted in each domain.

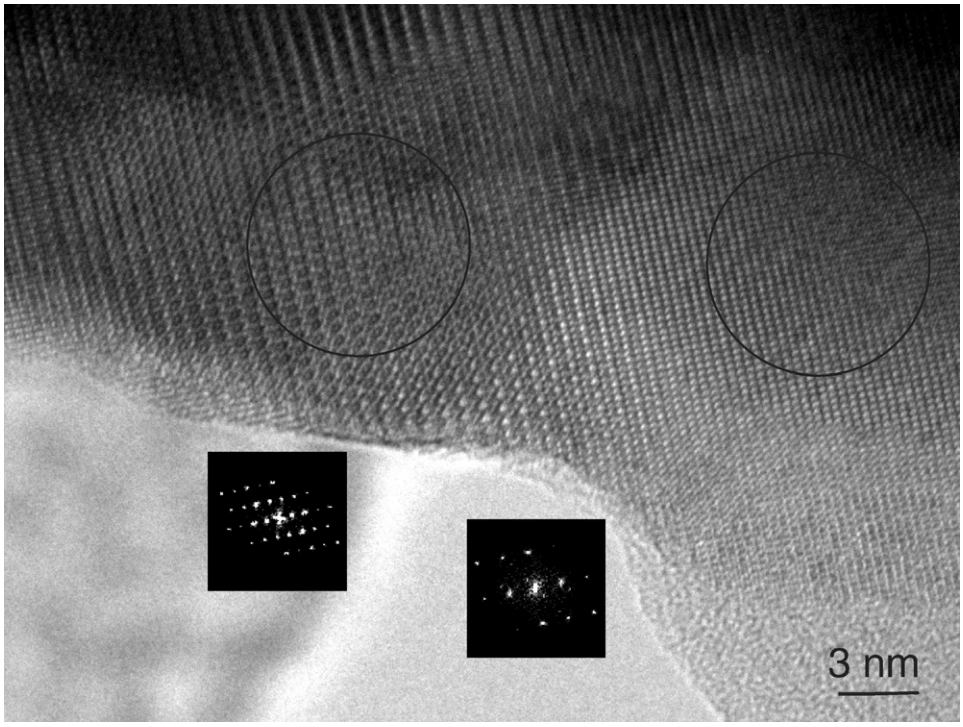

Fig. 8. An HREM image of a crystallite of brownmillerite-type $Sr_2Co_{2-x}Ga_xO_5$, $x = 0.3$ showing the intergrowth between two domains viewed along $[100]_{BM}$ and $[212]_{BM}$ which both corresponds to $[110]_p$ (p—perovskite sublattice). FFTs from the encircled areas are inserted. In the $[212]_{BM}$ region a weak modulation can be seen along $[04\bar{2}]_{BM} = [111]_p$. It gives rise to a weak satellite spot at $\mathbf{q} = \frac{1}{4}[111]^*_p\ [04\bar{2}]_{BM}$ in the FFT pattern and in the corresponding SAED pattern shown in Fig. 10.

to the length of the edge of the tetrahedra O2–O2. This leads to a decrease of the mostly ionic A–O bond distances and to the distortion of the tetrahedron via elongation of the edge connecting two octahedra from neighboring layers. The latter seems to be limited by the value of the tetrahedral angle O2–B–O2 (The angle 135–137° found in $Sr_2Co_{2-x}Ga_xO_5$, see Table 4, is large for a GaO_4 tetrahedra.) and further distortion of the structure

occurs via elongation of the axial octahedral B–O2 distances. For transition metal oxides an axial elongation of the octahedron would lead to an increased stability of the brownmillerite structure for compounds with Jahn–Teller cations, which is observed for e.g. Mn^{3+} (d^4) (Sr_2MnGaO_5 [6], Ca_2MnGaO_5 [7], Co^{2+} (d^7) ($La_2Co_2O_5$ [17]) and Cu^{2+} (d^9) ($LaSrCuGaO_5$ [18]). In these compounds, the transition metals preferentially occupy the octahedral position, while the second cation, if present is found in the tetrahedron. However, the brownmillerite structure is also found for cations having a symmetric electronic shell such as, e.g. Al^{3+} (d^0) and Fe^{3+} (d^5) in $Ca_2Fe_{2-x}Al_xO_5$, with $x = 0.57-1.0$, where Al^{3+} and Fe^{3+} cations are situated in both the octahedra and tetrahedra [19,20]. It has to be mentioned that a mixed occupancy is also found in Sr_2CoFeO_5 [22]. It is therefore not surprising that the non-Jahn–Teller cation Co^{3+} (d^6) in $Sr_2Co_{2-x}Ga_xO_5$ occupies both tetrahedral and octahedral sites although with a preference for the latter sites (see Table 3). This could partially explain the instability of the brownmillerite structure for $Sr_2Co_{2-x}Ga_xO_5$, $0.3 \leqslant x \leqslant 0.8$ since a tetrahedral coordination of Co^{3+} is not as stable as an octahedral one. Annealing in air at 1173 K leads to oxidation and disproportion of the $Sr_2Co_{2-x}Ga_xO_5$ and the formation of $Sr_6Co_5O_{15}$ containing only six-coordinated Co^{3+} and Co^{4+} and Co_3O_4 with Co^{2+} in tetrahedral site. The reason for the instability of the stoichiometric composition Sr_2GaCoO_5 is not clear. It could be due to the increasing amount of Ga^{3+} in the distorted octahedra, a coordination rarely observed for Ga^{3+}. Moreover, it is unlikely to be

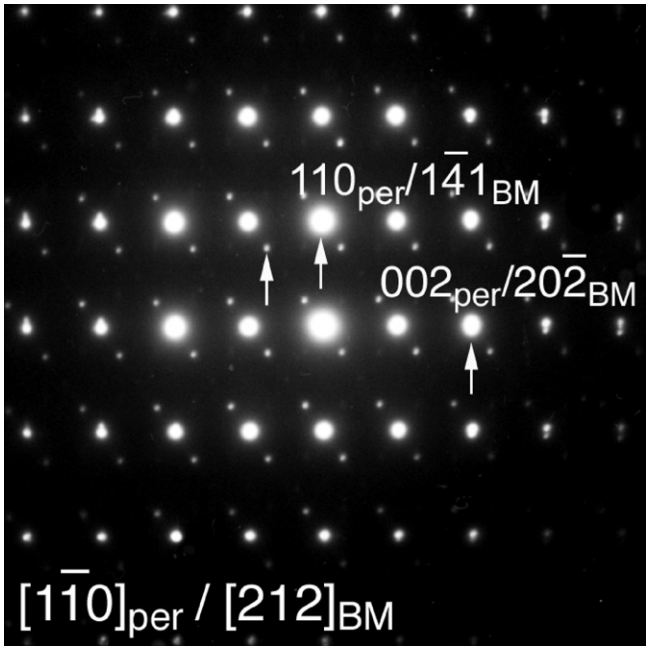

Fig. 9. SAED pattern of a domain of brownmillerite-type $Sr_2Co_{2-x}Ga_xO_5$, $x = 0.3$ viewed along $[212]_{BM}$. The corresponding HREM is shown in Fig. 10. In the SAED pattern there are satellite reflections at $\mathbf{q} = \frac{1}{4}\langle 111\rangle^*_p = \frac{1}{4}[04\bar{2}]^*_{BM}$.

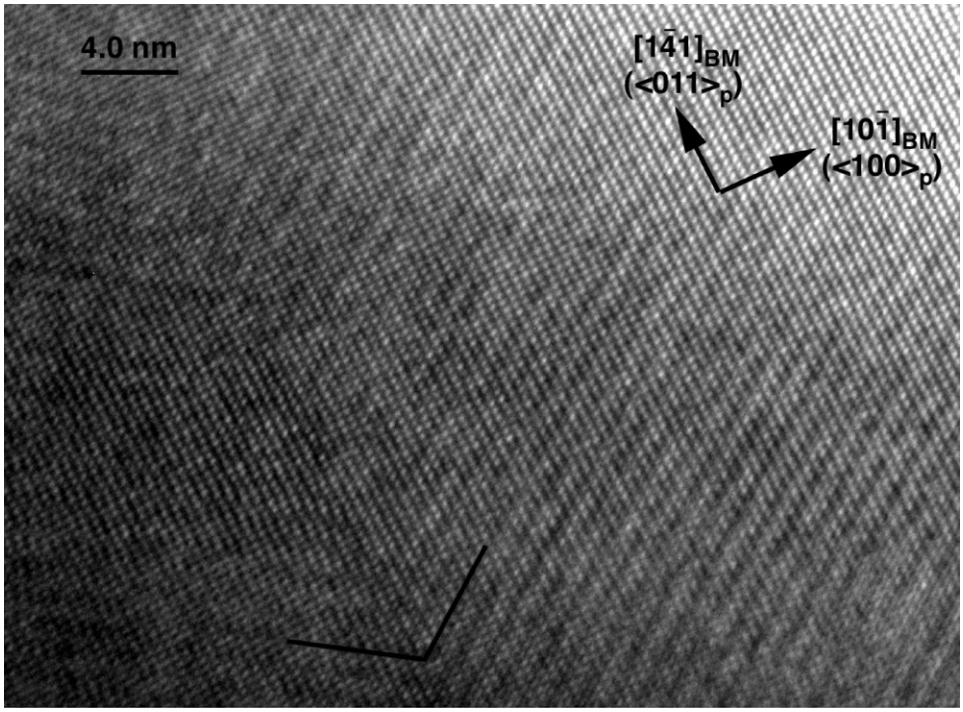

Fig. 10. A HREM image of brownmillerite-type $Sr_2Co_{2-x}Ga_xO_5$, $x = 0.3$ viewed along $[212]_{BM}$. A strong modulation along $[04\bar{2}]_{BM}$ can be seen. A FFT of the encircled area is inserted, showing that the modulation is commensurate with the basic brownmillerite structure with $\mathbf{q} = \frac{1}{4}[04\bar{2}]_{BM}$. ($\frac{1}{4}\langle 111\rangle_p$, p—perovskite substructure). In the area shown there is a twin boundary where the modulation is mirrored in plane parallel to $[\bar{1}01]_{BM} = \langle 100\rangle_p$.

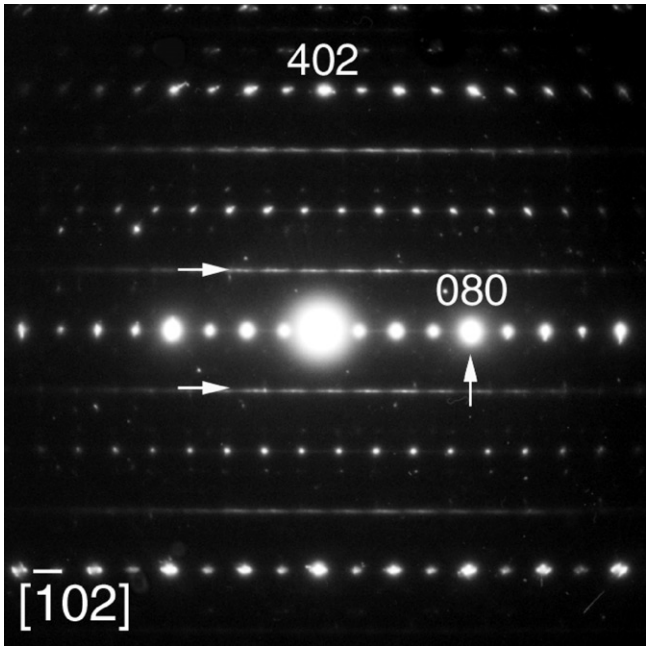

Fig. 11. (a) [201] zone axis selected area diffraction pattern of $Sr_2Co_{2-x}Ga_xO_5$, $x = 0.3$ along with streaking along [010] at $\mathbf{q} = \frac{1}{4}\langle 40 \pm 2 \rangle$.

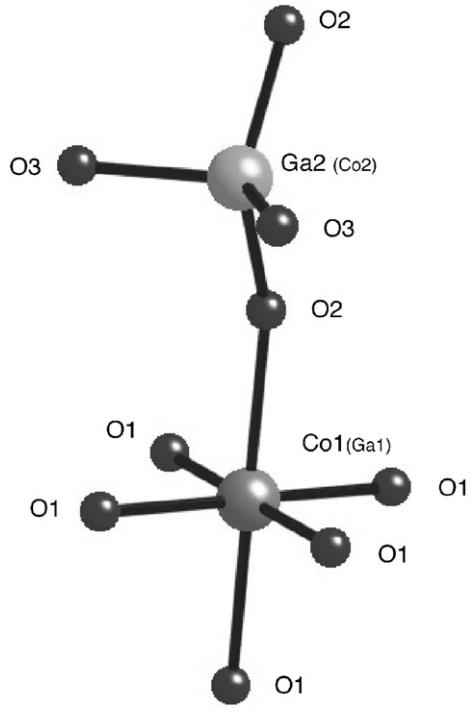

Fig. 12. Crystal structure of $Sr_2Co_{2-x}Ga_xO_5$, $x = 0.3$ showing one tetrahedron and one octahedron.

explained by the increasing of the distortion of the $Co^{3+}O_6$ octahedron with increasing gallium content, since changes in the interatomic distances are too small. For the $x = 0.3$ and 0.8 equatorial and axial Co–O

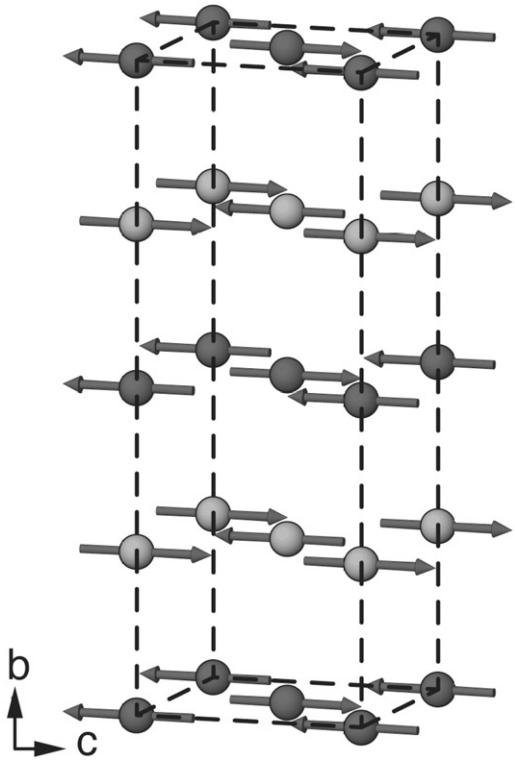

Fig. 13. Magnetic structure of $Sr_2Co_{2-x}Ga_xO_5$, $x = 0.3$. Dark spheres—Co1 in octahedra. Light spheres—Co2 in tetrahedra.

distances are 1.953(1), 2.254(3) and 1.959(1), 2.271(3) Å, respectively.

$Sr_2Co_{2-x}Ga_xO_5$ shows G-type antiferromagnetic order with the magnetic moments parallel to [001] direction, as in e.g. $Ca_2Fe_2O_5$ [21], see Fig. 13. This can be compared with other G-type antiferromagnetics among complex cobalt oxides with brownmillerite structure such as: $La_2Co_2O_5$ [17], with the moments oriented parallel to [101], while they are parallel to [100] or [001] in $Sr_2Co_2O_5$ [8]. In the latter case the exact orientations of the magnetic moments are not clear since no full structure refinement of $Sr_2Co_2O_5$ is available. The observed magnetic moments from the NPD study for both $x = 0.3$ and 0.8 compositions are lower (see Table 3) than expected for a high spin Co^{3+} d^6 ion. This has also been observed in $Sr_2Co_2O_5$ [9] and $Sr_2Co^{3+}FeO_5$ [22]: $\mu_{eff} = 3.3$–$3.4\mu_{BM}$ and $\mu_{eff}(Co1) = 3.2\mu_{BM}$ and μ_{eff} $(Co2) = 2.9\mu_{BM}$, respectively. The low values of the magnetic moments can be explained by the presence of disorder and non-magnetic Ga^{3+} in the structure. However, in this case it is difficult to speculate about the spin state of Co^{3+} in the structure. There is a direct correlation between the values of the magnetic moments, Néel temperature and Ga content in octahedral and tetrahedral sites. Magnetic moments for the Co^{3+} and T_N decreases with increasing Ga content (see Tables 2 and 3). Above the Néel temperature the magnetic moments decrease with increasing gallium

content (Table 2). However, for the compositions $x = 0.3$ and 0.5 the magnetic moments for Co^{3+} in the high-temperature region are higher than expected from spin-only moment for HS Co^{3+}. This indicates presence of a strong spin-orbital coupling, which is well known for cobalt in different oxidation states.

5. Conclusions

The substitution of Co^{3+} by Ga^{3+} in $Sr_2Co_2O_5$ leads to the formation of the brownmillerite-type phases in the composition range $0.3 \leqslant x \leqslant 0.8$. However, these phases are not stable below the temperature corresponding to the stability limit of the $Sr_2Co_2O_5$. The reason for the instability of the brownmillerite-type $Sr_2Co_{2-x}Ga_xO_5$, $0.3 \leqslant x \leqslant 0.8$ could be presence of Co^{3+} (d^6) in an unfavorable tetrahedral environment as revealed by structural refinements using NPD data of the $x = 0.3$ and 0.8 samples. These structural studies also show the presence of an unusually large dilation of the $Co^{3+}O_6$ octahedra caused by the structural peculiarities of the brownmillerite structure itself. A study of the magnetic structure of the prepared compounds shows that even the presence of 40% of non-magnetic Ga^{3+} in the structure did not destroy strong antiferromagnetic (AFM) interaction between Co^{3+}. However, there is a clear trend that the AFM coupling weakens with increasing gallium content as expected.

Transmission electron microscopy studies showed that the crystallites consisted of differently oriented brownmillerite domains with a common perovskite subaxis. The SAED patterns and the HREM images revealed the presence of disorder within the crystallites. In some of the crystallites satellite reflections were observed along $\mathbf{q} = \frac{1}{4}\langle 04\bar{2}\rangle_{BM} = \frac{1}{4}\langle 111\rangle_{p}$. However, further studies are needed to reveal the exact origin of this new type of modulation.

Acknowledgments

The authors thank Mr. L. Göthe for recording Guinier-Hägg X-ray powder diffraction photographs and to Mr. H. Rundlöf for neutron diffraction experiments. This research was partly supported by The Swedish Research Council, The Royal Swedish Academy of Sciences (KVA), Russian Foundation for Basic Research (grants no. 02-03-32990 and 02-02-06450) and Petroleum Research Foundation. S.M.K. is thankful to Mr. K. Mattenberger for the help with high temperature magnetic measurements.

References

[1] D.K. Smith, Acta Crystallogr. 15 (1962) 1146.
[2] A.A. Colville, S. Geller, Acta Crystallogr. B 27 (1971) 2311.
[3] A.R. Landa-Cánovas, S. Hansen, Cem. Conc. Res. 29 (1999) 679.
[4] S. Lambert, H. Leligny, D. Grebille, D. Pelliquin, B. Raveau, Chem. Mater. 14 (2002) 1818.
[5] A.M. Abakumov, M.G. Rozova, B.Ph. Pavlyuk, M.V. Lobanov, E.V. Antipov, O.I. Lebedev, G. van Tendeloo, O.L. Ignatchik, E.A. Ovtchenkov, Yu.A. Koksharov, A.N. Vasilév, J. Solid State Chem. 160 (2001) 353.
[6] A.J. Wright, H.M. Palmer, P.A. Anderson, C. Greaves, J. Mater. Chem. 12 (2002) 978.
[7] A.M. Abakumov, M.G. Rozova, B.Ph. Pavlyuk, M.V. Lobanov, E.V. Antipov, O.I. Lebedev, G. van Tendeloo, D.V. Sheptyakov, A.M. Balgurov, F. Bourée, J. Solid State Chem. 158 (2001) 100.
[8] T. Takeda, Y. Yamaguchi, H. Watanabe, J. Phys. Soc. Jpn. 33 (1972) 970.
[9] J.-C. Grenier, S. Ghobane, G. Demazeau, M. Pouchard, P. Hagenmuller, Mater. Res. Bull. 14 (1979) 831.
[10] W.T.A. Harrison, S.L. Hegwood, A.J. Jacobson, J. Chem. Soc. Chem. Commun. 1995 (1995) 1953.
[11] A.C. Larson, R.B. Von Dreele, General structure analysis system (GSAS), Los Alamos National Laboratory Report LAUR, 2000, pp. 86–748.
[12] R. Kilaas, MacTempas, www.totalresolution.com.
[13] JCPDS entry 31-1358.
[14] P. Berastegui, S. Hull, F.J. Garcia-Garcia, S.-G. Eriksson, J. Solid State Chem. 163 (2002) 119.
[15] R.D. Shannon, Acta Crystallogr. A 32 (1972) 258.
[16] C. Greaves, A.J. Jacobsen, B.C. Tofield, B.E.F. Fende, Acta Crystallogr. B 31 (1975) 641.
[17] O.H. Hansteen, H. Fjellvåg, B.C. Hauback, J. Solid State Chem. 141 (1998) 411.
[18] J.T. Vaughey, J.B. Wiley, K. Poeppelmeier, Z. Anorg. Allg. Chem. 598 (1991) 327.
[19] A. Colville, S. Geller, Acta Crystallogr. B 27 (1971) 2311.
[20] A. Colville, S. Geller, Acta Crystallogr. B 28 (1972) 3196.
[21] S. Geller, R.W. Grant, U. Gonser, M. Wiedresich, G.P. Espinosa, Phys. Lett. 20 (1966) 115.
[22] P.D. Battle, T.C. Gibb, P. Lightfoot, J. Solid State Chem. 76 (1988) 334.